# Ultrasensitive, Parity–Time-Symmetric Wireless Reactive and Resistive Sensors

Maryam Sakhdari, *Student Member, IEEE*, Mehdi Hajizadegan, *Student Member, IEEE*, Yue Li<sup>©</sup>, *Senior Member, IEEE*, Mark Ming-Cheng Cheng, Jonathan C. H. Hung, *Member, IEEE*, and Pai-Yen Chen, *Senior Member, IEEE* 

Abstract—We propose a new readout paradigm for enhancing the performance of wireless resistive and reactive sensors. Here, we consider a passive resistor-inductor-capacitor sensor that is inductively coupled to an active reader, with the equivalent circuit of the whole telemetry system obeying the space-time reflection symmetry or the parity-time (PT) symmetry. As inspired by PT-symmetric quantum systems, this circuit has a non-Hermitian effective Hamiltonian that commutes with the antilinear, combined PT operator, where P and T are parity-inversion and time-reversal operators. We demonstrate that the PT-symmetric wireless sensor system, when compared to conventional interrogation techniques using a passive coil antenna, may provide significantly improved quality factor (Q-factor), sensing resolution, and sensitivity in response to the sensor's reactance or resistance variation. Our results may have an impact on various wireless sensing, detection, and imaging systems, particularly for emerging micromachined sensors, miniature implants, wearables, and Internet-of-Things applications.

*Index Terms*—Wireless sensors and actuators, *LC* sensors, non-invasive sensors, parity–time symmetry, sensor telemetry.

## I. INTRODUCTION

ANY medical, industrial, and automotive applications require sensing of local physical or chemical quantities, where the wired connection between the sensor and the data acquisition system is not accessible. Representative examples include various bio-implants inside the human body (e.g. intraocular pressure sensors, intravascular pressure sensors, intracranial sensors, and tissue-characterization sensors [1]–[6]), pressure sensors on rotating components of vehicle, and sensing in harsh environments (e.g. corrosive media or high temperature [7], [8]). Telemetric sensing based on battery-free passive wireless sensors or radio-frequency identification (RFID) tags is perhaps one of the most viable ways to achieve the contactless and continuous measurement for the above mentioned applications. To date, a great

Manuscript received June 6, 2018; revised July 29, 2018; accepted August 30, 2018. Date of publication September 17, 2018; date of current version November 13, 2018. This work was supported by NSF ECCS-CCSS under Grant #1711409. The associate editor coordinating the review of this paper and approving it for publication was Prof. Dongsoo Har. (Corresponding author: Pai-Yen Chen.)

M. Sakhdari, M. Hajizadegan, and P.-Y. Chen are with the Department of Electrical and Computer Engineering, The University of Illinois at Chicago, Chicago, IL 60607 USA (e-mail: pychen@uic.edu).

Y. Li is with the Department of Electronic Engineering, Tsinghua University, Beijing 100084, China, and also with the Department of Electrical and Systems Engineering, University of Pennsylvania, Philadelphia, PA 19104 USA. M. M.-C. Cheng is with Wayne State University, Detroit, MI 48202 USA. J. C. H. Hung is with Maxim Integrated Corp., Dallas, TX 75240 USA. Digital Object Identifier 10.1109/JSEN.2018.2870322

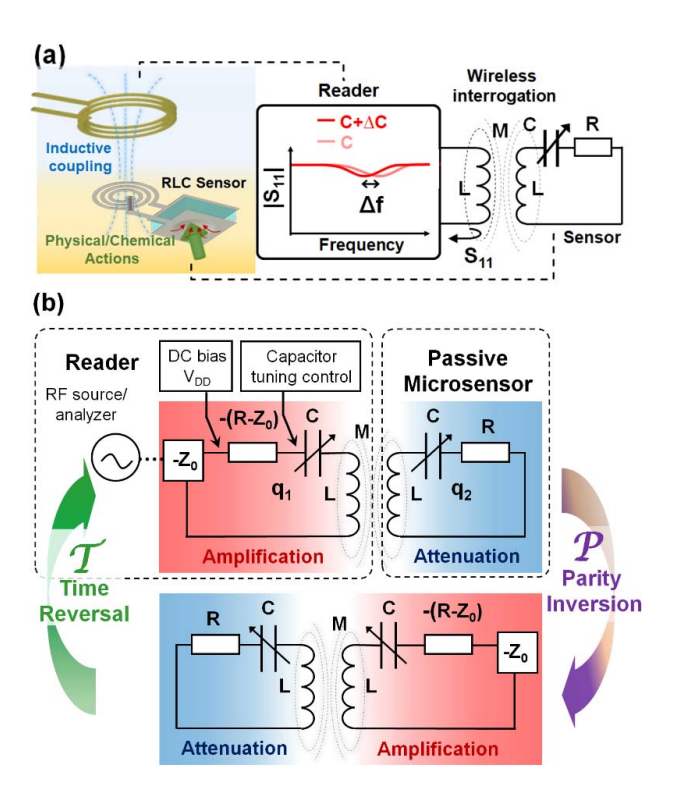


Fig. 1. (a) Schematics of a wireless passive *RLC* sensor, inductively coupled to a coil reader, and its equivalent circuit model. (b) Equivalent-circuit expression of the *PT*-symmetric wireless sensor system.

number of low-cost and low-profile wireless sensors have been proposed to measure miscellaneous quantities, such as temperature [8], [9], pressure [1], [7], [10]–[12], liquid volume [13], [14], humidity [15], [16], mechanical strain [17], and chemical reactions (e.g., chemresistive sensors). Most of these sensing devices are based on the passive *RLC* tank, where the quantity to be measured may change the effective resistance or effective capacitance/inductance of the sensor, resulting in the resonance frequency shift. Typically, a reader coil antenna is used to measure the frequency response of the wireless sensor through the inductive coupling, as illustrated in Fig. 1a.

Although, so far, many research efforts have been focused on the design and fabrication of miniature functional sensors, very limited effort has been made to develop a more robust and sensitive wireless readout technique. However, existing readout methods for passive wireless sensors still face several challenges. For instance, sensitivity and minimum detection

range of the miniature wireless sensors (e.g. integrated circuit piezoelectric or ICP sensors) usually suffer from the small resonance frequency shift and the low Q-factor, resulting from limited device dimensions, skin-effect and Eddy-current losses, and background absorption (e.g. human tissues and organs at high frequencies). In general, an effective resistance taking into account the total power dissipation must be introduced into the RLC tank, as shown in Fig. 1a. In this context, negative-resistance-based oscillators have been proposed for enhancing the resolution and the Q-factor of microwave-resonator sensors, of which the sharp transmission peak ( $S_{21}$ ) is achieved with the effect of loss compensation [18]–[20].

In this work, we present a new wireless readout technique based on the concept of *PT*-symmetry, which may significantly enhance the sensitivity and the detection limit of transformer-based sensors. Figure 1b shows the equivalent circuit of the proposed *PT*-symmetric wireless sensor system, where the passive wireless functional sensor, modeled by an equivalent *RLC* tank circuit, is inductively coupled to an active -RLC reader circuit. The whole telemetry system fulfills the spatial-inversion and time-reversal symmetry, so-called *PT*-symmetry [21]. In the following, we will theoretically and experimentally investigate the performance and critical operation conditions of the proposed *PT*-symmetric wireless sensors, which can provide loss compensation and optimal sensing performance.

#### II. PT-SYMMETRIC TELEMETRIC SENSOR SYSTEMS

The concept of PT-symmetry originates from the quantum mechanics, where a non-Hermitian Hamiltonian can have real eigenfrequencies, if the Schrödinger system is invariant under operations of spatial reflection  $\mathcal{P}$  and time reversal  $\mathcal{T}$  [21]. Thanks to formal similarities between Schrödinger and Helmholtz equations, PT-symmetry can be experimentally demonstrated in electromagnetic systems with balanced gain and loss [22]-[28], including transmission-line networks, coupled waveguides/cavities, and lumped-element circuits [29]–[34]. As illustrated in Fig. 1b, a PT-symmetric electronic circuit can be made by pairing the -RLC and RLC tanks, correspondingly responsible for the amplification and attenuation of RF signal. When a RF source, such as a frequency synthesizer based on the negative-resistance device, excites this dimer circuit, a negative generator impedance  $-Z_0$  must be included in the coupled-mode (closed-loop) analysis [35]. This is because while a resistor renders energy dissipation, a negative resistor implies an energy source. Therefore, for balancing the net gain and loss, a negativeresistance converter (NRC) with a resistance of  $-(R-Z_0)[\Omega]$ must be used in the -RLC tank (which is connected to the RF signal generator/analyzer representing  $-Z_0$ ).

Applying Kirchhoff's laws to the circuit in Fig. 1b leads to the following set of equations:

$$\frac{d^2q_1}{d\tau^2} = -\frac{1}{1-\kappa^2}q_1 + \frac{\kappa}{1-\kappa^2}q_2 + \frac{1}{\gamma(1-\kappa^2)}\dot{q}_1 + \frac{\kappa}{\gamma(1-\kappa^2)}\dot{q}_2$$
 (1a)

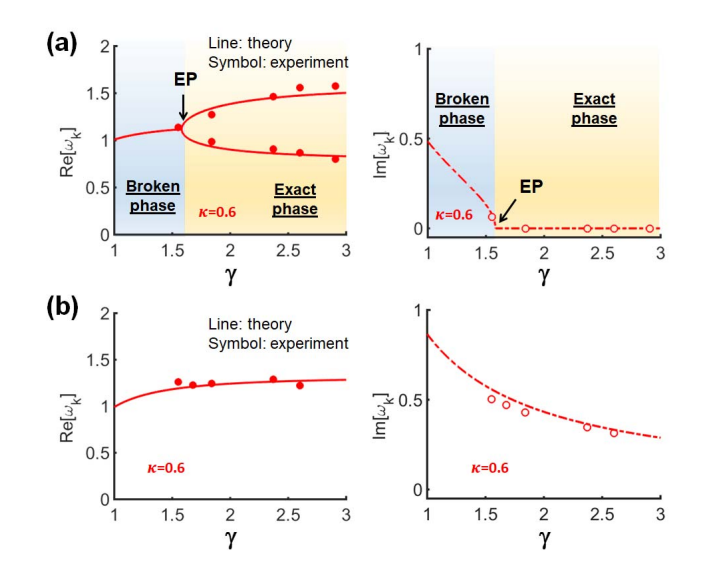


Fig. 2. (a) Real (left) and imaginary (right) eigenfrequency versus the non-Hermiticity parameter  $\gamma$  for the *PT*-symmetric circuit in Fig. 1b. (b) is similar to (a), but for measurement results obtained by the micro-coil reader shown in Fig. 1a. Here, eigenfrequencies are in units of  $\omega_0$ .

$$\frac{d^{2}q_{2}}{d\tau^{2}} = \frac{\kappa}{1 - \kappa^{2}} q_{1} - \frac{1}{1 - \kappa^{2}} q_{2} - \frac{\kappa}{\gamma (1 - \kappa^{2})} \dot{q}_{1} - \frac{1}{\gamma (1 - \kappa^{2})} \dot{q}_{2},$$
(1b)

where  $q_1$  ( $q_2$ ) corresponds to the charge stored on the capacitor in the amplifying (attenuating) tank,  $\tau \equiv \omega_0 t$ , the natural frequency of an RLC tank  $\omega_0 = 1/\sqrt{LC}$ , the dimensionless gain-loss parameter or the non-Hermiticity parameter  $\gamma = R^{-1}\sqrt{L/C}$ ,  $\kappa = M/L$  is the coupling strength between the -RLC and RLC tanks, M is the mutual inductance, and  $0 \le \kappa \le 1$ ; here all frequencies are measured in units of  $\omega_0$ . We find that Eq. (1) remains unchanged under the combined  $\mathcal{P}$  ( $q_1 \leftrightarrow q_2$ ) and  $\mathcal{T}$  ( $t \leftrightarrow -t$ ) transformations. Further, Eq. (1) can be written in the Liouvillian formalism as [36]:

$$\mathcal{L} = \begin{pmatrix} 0 & 0 & 1 & 0 \\ 0 & 0 & 0 & 1 \\ -\frac{1}{1-\kappa^2} & \frac{\kappa}{1-\kappa^2} & \frac{1}{\gamma(1-\kappa^2)} & \frac{\kappa}{\gamma(1-\kappa^2)} \\ \frac{\kappa}{1-\kappa^2} & -\frac{1}{1-\kappa^2} & -\frac{\kappa}{\gamma(1-\kappa^2)} & -\frac{1}{\gamma(1-\kappa^2)} \end{pmatrix},$$
(2)

where  $\Phi \equiv (q_1, q_2, \dot{q}_1, \dot{q}_2)^T$ . An effective Hamiltonian can be defined as  $H_{eff} = i \mathcal{L}$ , which takes a non-Hermitian form and is symmetric with respect to generalized  $\mathcal{P}\mathcal{T}$  transformations:

$$\mathcal{P} = \begin{pmatrix} \sigma_{x} & 0 \\ 0 & \sigma_{x} \end{pmatrix}, \quad \mathcal{T} = \begin{pmatrix} \mathbf{I} & 0 \\ 0 & -\mathbf{I} \end{pmatrix} \mathcal{K}, \tag{3}$$

 $\sigma_x$  is the Pauli matrix, **I** is an  $2 \times 2$  identity matrix, and  $\mathcal{K}$  conducts the operation of complex conjugation.  $H_{eff}$  commutes with  $\mathcal{PT}$ , namely  $\left[\mathcal{PT}, H_{eff}\right] = 0$ , which implies that  $H_{eff}$  and  $\mathcal{PT}$  share the same set of eigenstates.

After the substitution of time-harmonic charge distributions  $q_n = A_n e^{i\omega\tau}$ , eigenfrequencies for this *PT*-symmetric circuitry can be obtained from the eigenvalue equation,  $(H_{eff} - \omega_k \mathbf{I})\Phi_k = 0$  and k = 1, 2, 3, 4, as functions of the non-Hermiticity parameter  $\gamma$  and the coupling strength  $\kappa$ :

$$\omega_{1,2,3,4} = \pm \sqrt{\frac{2\gamma^2 - 1 \pm \sqrt{1 - 4\gamma^2 + 4\gamma^4 \kappa^2}}{2\gamma^2 (1 - \kappa^2)}},$$
 (4)

Although there are four normal modes, there is redundancy and only two distinct modes are necessarily considered because positive and negative eigenfrequencies of equal magnitude are essentially identical. The complex eigenfrequencies evolve with  $\gamma$ , showing three distinct regimes of behavior. As can be seen in Fig. 2a, the eigenfrequencies undergo a bifurcation process and branch out into the complex plane at the exceptional point (or the spontaneous PT-symmetry breaking point):

$$\gamma_{EP} = \frac{1}{\kappa} \sqrt{\frac{1 + \sqrt{1 - \kappa^2}}{2}}.$$
 (5)

In the parametric region  $\gamma \in [\gamma_{EP}, \infty]$ , eigenfrequencies are purely real  $(\gamma \in \mathbb{R})$  and  $\mathcal{P}T\Phi_k = \Phi_k$  such that the PT-symmetry is exact. Moreover, if one seeks only purely real solutions, there is redundancy because positive and negative eigenfrequencies of equal magnitude are essentially identical. The motion in this exact PT-symmetric phase is oscillatory at the two (purely real) eigenfrequencies. At the exceptional point  $\gamma_{EP}$ , eigenfrequencies undergo a bifurcation process and branch out into the complex plane, and thus the PT-symmetry is spontaneously broken. The region  $\gamma \in [\gamma_c, \gamma_{EP}]$  is known as the broken PT-symmetric phase, where eigenfrequencies become two complex conjugate pairs  $(\gamma \in \mathbb{C})$ . In this region,  $\mathcal{P}T\Phi_k \neq \Phi_k$  and the PT-symmetry is broken. Another crossing between the pairs of degenerate frequencies (and another branching) occurs at the lower critical point:

$$\gamma_c = \frac{1}{\kappa} \sqrt{\frac{1 - \sqrt{1 - \kappa^2}}{2}}.\tag{6}$$

In the sub-critical region  $\gamma \in [0, \gamma_c]$ ,  $\omega_k$  become purely imaginary and, therefore, the modes have no oscillatory part and simply blow up or decay away exponentially, corresponding to the over-damped/amplified mode. Finally, we note that in the loss (gain)-less scenario ( $\gamma \to \infty$ ), two frequency pairs are given by  $\omega_{1,2,3,4} = \pm 1/\sqrt{1 \pm \kappa}$ . These modes are associated with a pair of double-degenerate frequencies  $\omega_k = \pm 1$  for a single isolated LC tank with  $\kappa = 0$ .

Figures 3a and 3b show the frequency responses of reflection ( $\Gamma$ ), as functions of  $\gamma$  and the normalized frequency  $\omega$  [ $\omega_0$ ], for the conventional wireless sensor system [1]–[17] (which uses a coil antenna with inductance L to interrogate the passive sensor [Fig. 1a]), and the PT-symmetric one (which consists of a -RLC tank to communicate with the same sensor [Fig. 1b]); here, we assume that the coupling strength  $\kappa=0.6$  and the input impedance of the RF source (e.g. a vector network analyzer or VNA)  $Z_0=0.33R$ . We find that resonant reflection dips in Fig. 3b are in consistent with the eigenfrequency analysis in Fig. 2a: (1) if  $\gamma<\gamma_c$ , there

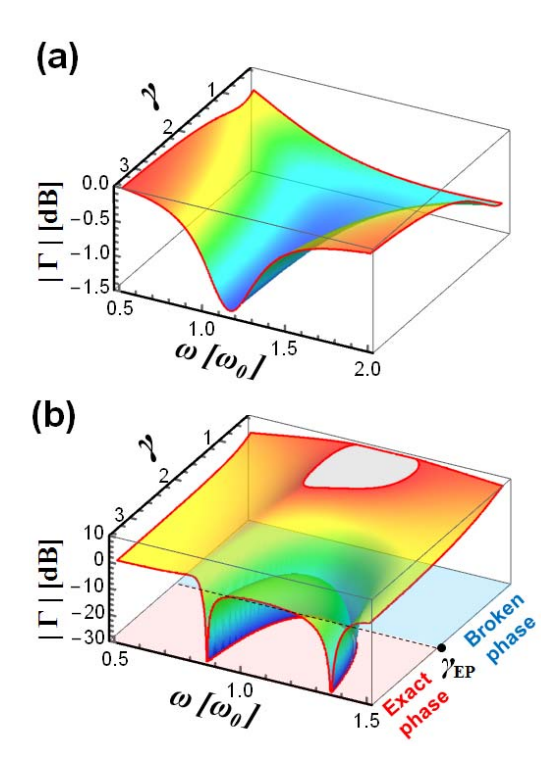


Fig. 3. Contours of reflection coefficient, as a function of the normalized operating frequency and the non-Hermiticity parameter, for the circuit of (a) the conventional wireless sensor system [Fig. 1(a)] and (b) the *PT*-symmetric one [Fig. 1(b)]; here the coupling strength  $\kappa=0.6$  and the input impedance of the RF source  $Z_0=0.33~R$ .

is no clear resonant peak, but a purely amplification or decay phenomenon; (2) if  $\gamma \in [\gamma_c, \gamma_{EP}]$ , a broadband resonance is obtained, as the system operates in the broken *PT*-symmetry phase; (3) if  $\gamma > \gamma_{EP}$ , the exact *PT*-symmetry phase yields two real eigenfrequencies, resulting in sharp reflection dips. Comparing the conventional fully-passive wireless sensing scheme and the *PT* one, it is seen that the proposed approach may offer superior sensitivity in terms of resonance frequency shift due to perturbations in  $\gamma$ , modulation depth, and spectral resolution; here,  $\gamma$  is a function of the sensor's effective resistance, capacitance, and inductance that could be tuned by physical or chemical parameters to be sensed.

# III. IMPLEMENTATION AND CHARACTERIZATION OF WIRELESS CAPACITIVE SENSORS

To validate the theoretical results in Section II, we have built a PT-symmetric RF circuit that resembles practical wireless sensor systems. For example, many medical and industrial pressure sensors are based on the capacitance change due to the mechanical deflection or the variation of dielectric constant [8], [10]. In order to mimic a passive wireless capacitive sensor, we have made an onboard series RLC tank [Fig. 1a], consisting of a variable capacitor (BBY40: C=2-32 pF), a resistor (MNR02JR-0402:  $R=150\pm0.5\%~\Omega$ ), and a microstrip coil ( $L=0.3~\mu{\rm H}$ ) [37]. To suit the PT-symmetric circuit topology in Fig. 1b, the reader may need to be equipped with a negative resistor -R, which can be realized by a NRC that pulls in power to the circuit, rather than dissipating it like a resistor. Hence, the active reader is a -RLC tank that has

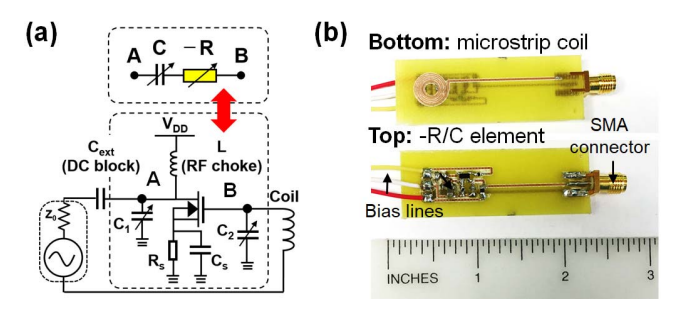


Fig. 4. (a) Circuit diagram for the active reader consisting of a NRC, which is equivalent to a lumped negative resistor and (b) its practical implementation using the printed circuit board technique.

the same effective capacitance and inductance as those of the passive *RLC* tank (i.e., sensor).

Figures 4a and 4b respectively show the circuit diagram and the photograph of the positive-feedback Colpitts-type NRC [37]–[44], which is equivalent to a negative resistor connected in series with a capacitor. Both effective -R and C are tunable (via the external DC bias), stabilized, and nearly non-dispersive over a wide frequency range. For the NRC circuit in Fig. 4a, if the transistor's transconductance  $g_m \gg \omega C_{gd}$ ,  $\omega C_{gs}$  ( $C_{gd}$  and  $C_{gs}$  are the gate-drain and gate-source capacitances), the equivalent impedance of the NRC is approximately given by:

$$Z_{eq} \approx -\frac{g_m}{\omega^2 C_1 C_2} - j \left( \frac{1}{\omega C_1} + \frac{1}{\omega C_2} \right),$$
 (7)

where the real and imaginary parts correspond to the negative resistance and the capacitance. The negative resistance value can be controlled by the DC offset voltages of the transistor (RF n-channel MOSFET: SOT-143). The effective capacitance of NRC is also tunable, if two voltage-controlled varactors  $C_1$  and  $C_2$  are used.

We have designed and manufactured an active onboard reader (-RLC tank) to wirelessly interrogate the RLC tank that simulates the capacitive wireless sensor. Once the capacitance of the RLC tank is varied, the effective capacitance of the reader is adjusted accordingly to maintain the PT-symmetry condition. The inset of Fig. 5 shows our measurement setup, where the reader and the pseudo-sensor are separated by an air gap of 5 mm, yielding a coupling strength  $\kappa = 0.6$ . Figures 5a and 5b present evolutions of the reflection spectrum with different capacitance values for the conventional [Fig. 1a] and PT-symmetric [Fig. 1b] wireless sensor systems, respectively; here, the effective capacitance C of the RLC tank is varied from 2 pF to 7 pF, corresponding to the change of  $\gamma$  from 2.905 to 1.553. As can be seen in Fig. 5, experimental (solid lines) and theoretical (dashed lines) results agree quite well. The slight difference between the theory and experiment can be further improved by flattening the frequency response of NRC, which, for instance, could be achieved with the cross-coupled transistor pair [37]–[44] and the on-chip design. In this case, the non-Hermiticity parameter of the PT system,  $\gamma$ , as a function of C, determines whether the PT-symmetry is exact or broken. If  $\gamma < \gamma_{EP}$ , the system will operate in the broken PT-symmetric phase and vice versa. We have retrieved

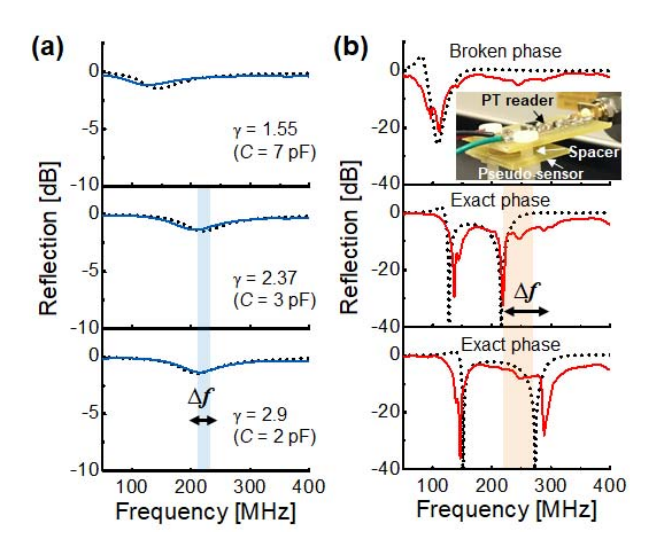


Fig. 5. Measured reflection coefficient for a passive *RLC* pseudo-sensor with an effective resistance  $R=150~\Omega$  and an effective inductance L=300~nH, which is inductively coupled by (a) the conventional coil-antenna reader shown in Fig. 1a, and (b) the active reader (-RLC tank in Fig. 1b) that accomplishes the *PT*-symmetric electronic system. The effective capacitance C of the *RLC* sensor is varied from 7 pF to 2 pF. Here, solid and dashed lines represent experimental and theoretical results, respectively.

from measurement results [36] the complex eigenfrequency versus γ for both fully-passive and active wireless sensor systems in Fig. 5. Results are highlighted as dots in Fig. 2, which show excellent agreement with the theory. It is seen from Figs. 2 and 5 that by sweeping C from high to low values (or, effectively, sweeping  $\gamma$  from low to high values), the PT-symmetric telemetry system may evolve from the broken symmetry phase to the exact symmetry phase. The exact PT-symmetric phase results in real eigenfrequencies, associated with narrowband and sharp-peaked resonances. On the other hand, the broken PT-symmetry phase exhibits complex eigenfrequencies, associated with a weak and broad resonance. From Fig. 5, it is evidently seen that the PT-symmetric wireless readout technique, when operated in the exact symmetry phase, may enable much sharper reflection dips and greater Q-factor than the fully-passive readout technique.

It is worth mentioning that the PT-symmetric circuit may provide not only the loss compensation effect and the high-Q resonance, but also the enhanced sensitivity, in terms of the resonance frequency shift in response to the sensor's impedance perturbation. As can be seen in Figs. 2a and 2b, under the same values of  $\Delta \gamma$ , the PT-symmetric telemetric system shows a more dramatic eigenfrequency bifurcation, compared to the conventional full-passive one (whose eigenfrequency variation is a flat line after being normalized by  $\omega_0 = 1/\sqrt{LC}$ ). The sensitivity enhancement is particularly obvious around the singular exceptional point  $\gamma_{EP}$ , where largely bifurcating eigenfrequencies (resonance frequency) can lead to an ultrahigh sensitivity [45], [46]. Such a property has been utilized to enhance the sensitivity of optical sensors based on amplifying and lossy microcavities [45], [46]. We note that if the negative resistor in the reader is replaced by a normal resistor of the same absolute resistance value, the PT-symmetry is no more valid and the complex-valued

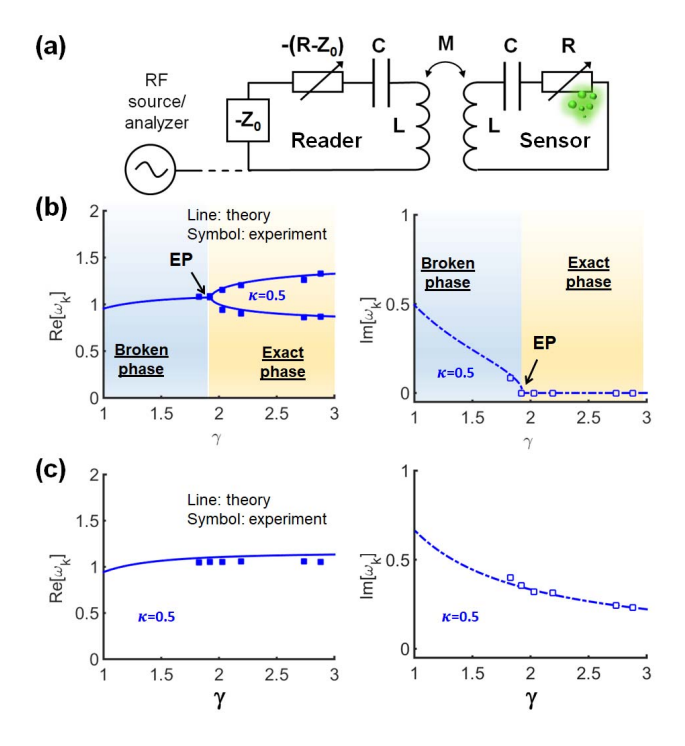


Fig. 6. (a) Schematics of the PT-symmetric wireless resistive sensor system. (b) Real (left) and imaginary (right) eigenfrequency versus the non-Hermiticity parameter  $\gamma$  for the PT-symmetric circuit in (a). The resistance of the pseudo RLC sensor is varied from 190  $\Omega$  to 300  $\Omega$ , corresponding to the change of  $\gamma$  from 2.8 to 1.9. (c) is similar to (b), but for measurement results obtained by the micro-coil reader shown in Fig. 1a. Here, eigenfrequencies are in units of  $\omega_0$ .

eigenfrequency results in a broad (low-Q) resonance (not shown here for saving some space) and low sensitivity to perturbations of  $\gamma$ .

# IV. IMPLEMENTATION AND CHARACTERIZATION OF WIRELESS RESISTIVE SENSORS

Recently, there has been substantial investigation and research in wireless (bio-)chemical sensors based on the chemiresistor (i.e., chemically-tuned variable resistor). Particularly, nanomaterials (e.g., graphene [47], [48]) has been a recent thrust in micro/nano-sensor development. However, due to the large electrical resistance of chemiresistor, these resistive sensors typically exhibit low Q-factor and imperceptible resonance frequency shift. In this work, we also apply the concept of PT-symmetric telemetry to improve the sensing performance of wireless resistive sensors. In this scenario, a variable resistor is connected in series with a capacitor and an inductor, forming a passive RLC tank. The sensor is inductively coupled to an active reader based on a -RLC tank, as shown in Fig. 6a. For the proof-of-concept demonstration, we used an onboard RLC tank with a variable resistor to simulate the resistance variation caused by, for example, chemical reactions in a chemiresistor. The series *RLC* tank is built by a microstrip coil ( $L \approx 0.6 \mu H$ ), a capacitor (BBY40:  $C \approx 2$  pF), and a variable resistor (MNR02JR-0402:  $R = 150 \sim 300 \pm 0.5\% \Omega$ ). The active reader is similar to the one used in Section III, of which the effective negative resistance is tuned by the external DC bias. When the

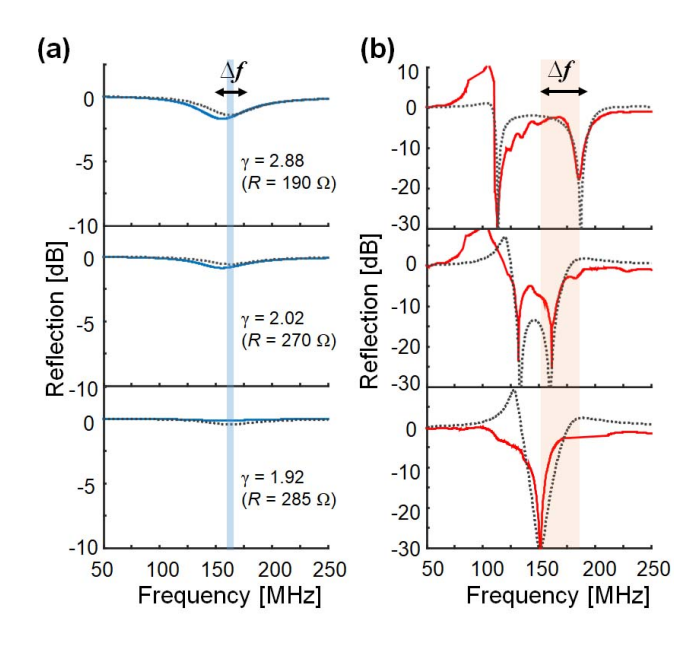


Fig. 7. Measured reflection coefficient for a (pseudo) *RLC* sensor with effective capacitance C=2 pF and effective inductance L=600 nH, which is wirelessly read by (a) the conventional coil-antenna reader shown in Fig. 1a, and (b) the active reader (-RLC tank in Fig. 6b). The effective resistance R of the pseudo RLC sensor is varied from 190  $\Omega$  to 285  $\Omega$ .

active reader (-RLC tank) is used to wirelessly interrogate the pseudo resistive sensor (RLC tank), the PT-symmetric telemetry system can be achieved, with its equivalent circuit shown in Fig. 6a.

Figure 6b presents the theoretical (solid lines) and experimental (dots) results for the complex eigenfrequency as a function of the non-Hermiticity parameter  $\gamma$ , which is varied by adjusting the effective resistance of the *RLC* tank sensor. Here, we find a good agreement between experimental and simulation results. Similar to the case of *PT*-symmetric wireless capacitive sensor [Fig. 2], there exists two distinct regimes of behavior divided by the exceptional point. As can be seen in Fig. 6b, around the exceptional point, the real eigenfrequencies become ultrasensitive to perturbation of the sensor's effective resistance. Figure 6c is similar to Fig. 6b, but for the fully-passive wireless sensing scheme using a simple microcoil reader. In this case, the eigenfrequency is complex-valued and insensitive to the change in  $\gamma$  (or R of the sensor).

Figures 7a and 7b present evolutions of the reflection spectrum for the fully-passive and *PT*-symmetric wireless sensor systems in Fig. 6, respectively. In both cases, measurements results (solid lines) are in good agreement with theory (dashed lines). As can be seen in Fig. 7, in the *PT*-symmetric telemetry system, the real eigenfrequncies give rise to sharp and high-*Q* reflection dips, even though the sensor's effective resistance is large. However, the passive micro-coil reader only achieves a weak resonance with a broad linewidth. Again, our measurement results demonstrate that a wireless sensor system engineered into the *PT*-symmetric dimer can provide superior sensitivity and detectivity, as it achieves not only higher spectral resolution and greater modulation depth, but also more sensitive frequency responses associated with the bifurcation

effect near the exceptional point. Fundamentally different from conventional loss-compensation resonator circuit, where -R and R components are in direct contact [18]–[20], [41], [42], in our PT-symmetric telemetry system, the balanced gain and loss are wirelessly interacted, thus offering a promising route for improving the performance of the wireless reactive and resistive sensors (e.g., without the need of active component and power source in the sensor). Most importantly, the PT-synthetic circuit topology can significantly enhance the sensitivity in terms of the resonance frequency shift under reactive and resistive perturbations.

### V. FUNDAMENTAL LIMIT OF SENSITIVITY

In this section, we will study the fundamental limit of sensitivity of PT-symmetric telemetric sensors. Of particular interest is the strong coupling regime. In an extreme case, if  $\kappa=1$ , the critical and exceptional points have the same value:  $\gamma_c=\gamma_{EP}=1/\sqrt{2}$ , and the degenerate eigenfrequencies become  $\pm i\infty$ , owning to the overlap between these two points. As  $\kappa$  approaches (but less than) unity and  $\gamma\gg\gamma_{EP}$ , the four eigenfrequencies expressed in units of  $\omega_0$  are:

$$\omega_{1,2,3,4} \simeq \pm \frac{1}{\sqrt{1 \pm \kappa}},\tag{8}$$

which merge at the exceptional point:

$$\omega_{EP} = \pm \frac{1}{4\sqrt{1 - \kappa^2}}.\tag{9}$$

When the exceptional point is taken as a reference, the possible bifurcation range is given by:

$$\Delta\omega_{+} \in \left[0, (1-\kappa)^{-1/2} - \left(1-\kappa^{2}\right)^{-1/4}\right];$$
 (10a)

$$\Delta\omega_{-} \in \left[ (1+\kappa)^{-1/2} - \left(1-\kappa^{2}\right)^{-1/4}, 0 \right], \quad (10b)$$

where  $\Delta\omega_+$  and  $\Delta\omega_-$  are variations in the upper and lower branches of eigenfrequencies. From Eq. (10), one can readily understand that if the coupling strength approaches one,  $\Delta\omega_+$  and  $\Delta\omega_-$  tend to:  $\Delta\omega_+ \in [0,\infty]$  and  $\Delta\omega_- \in [-\infty,0]$ . In this case, largely bifurcating eigenfrequencies are obtained around the exceptional point, implying that even a small perturbation of  $\gamma$  could lead to considerably shifted resonance frequencies. It is worth mentioning that the bifurcating rate of eigenfrequencies, related to the sensitivity of wireless *RLC* sensor, increases with increasing the coupling strength (not shown here). However, the coupling strength (or the mutual inductance between two coils) has its own limit. In practice, for two tightly coupled planar coils, it is difficult to achieve a large  $\kappa$  that is close to one.

In another extreme case, if  $\kappa=0$ , the critical and exceptional points are:  $\gamma_c=1/2$  and  $\gamma_{EP}\to\infty$ , which are far apart from each other. In the weak coupling regime (i.e.,  $\kappa\ll1$ ), if  $\gamma\gg\gamma_c$ , the four eigenfrequencies expressed in units of  $\omega_0$  can be derived as:

$$\omega_{1,2,3,4} \simeq \pm 1 \pm \frac{\kappa}{2} \sqrt{1 - \frac{1}{(\kappa \gamma)^2}}.$$
 (11)

If  $\gamma \gg \gamma_{EP}$ , the four eigenfrequencies become:

$$\omega_{1,2,3,4} \simeq \pm 1 \pm \frac{\kappa}{2},$$
 (12)

which degenerate into  $\omega_{EP} \simeq \pm 1$  at the exceptional point. Hence, when taking the exceptional point as a reference, the maximum range of the eigenfrequency shift is given by:

$$\Delta\omega_{+} \in [0, \kappa/2]; \tag{13a}$$

$$\Delta\omega_{-} \in [-\kappa/2, 0]. \tag{13b}$$

If  $\kappa \ll 1$ , the bifurcation effect is rather weak and thus low sensitivity is obtained. Based on the above discussions, we can conclude that the sensitivity is proportional to the coupling strength. If the coupling strength approaches the singular point ( $\kappa = 1$ ), at which  $\gamma_c$  and  $\gamma_{EP}$  overlap, the effect of sensitivity enhancement due to the bifurcation effect is particularly obvious.

#### VI. CONCLUSIONS

We have put forward the concept and practical designs of the PT-symmetric telemetry system for enhancing the sensitivity and detection limit of *RLC*-based passive wireless sensors. Specifically, the equivalent circuit of this wireless sensor system is tailored to fulfill the spatial-inversion and time-reversal symmetry, so-called PT-symmetry. We have first theoretically studied different PT phases and critical conditions for obtaining the optimal sensing performance. Then, we have experimentally demonstrated the possibility of using the PT-symmetry concept to wirelessly read the (lossy) capacitive and resistive sensors, with high spectral resolution and high sensitivity. The proposed wireless sensing technique is potentially revolutionary, as it may be beneficial to a plurality of environmental, infrastructural, wearable, and implantable wireless sensors, as well as emerging applications in the fields of RFIDs and IoTs.

### REFERENCES

- [1] P.-J. Chen, D. C. Rodger, S. Saati, M. S. Humayun, and Y.-C. Tai, "Microfabricated implantable parylene-based wireless passive intraocular pressure sensors," *J. Microelectromech. Syst.*, vol. 17, no. 6, pp. 1342–1351, Dec. 2008.
- [2] L. Brancato, G. Keulemans, T. Verbelen, B. Meyns, and R. Puers, "An implantable intravascular pressure sensor for a ventricular assist device," *Micromachines*, vol. 7, no. 8, p. 135, Aug. 2016.
- [3] M. Yvanoff and J. Venkataraman, "A feasibility study of tissue characterization using LC sensors," *IEEE Trans. Antennas Propag.*, vol. 57, no. 4, pp. 885–893, Apr. 2009.
- [4] L. Y. Chen et al., "Continuous wireless pressure monitoring and mapping with ultra-small passive sensors for health monitoring and critical care," Nature Commun., vol. 5, p. 5028, Oct. 2014.
- [5] M. W. A. Khan, T. Björninen, L. Sydänheimo, and L. Ukkonen, "Remotely powered piezoresistive pressure sensor: Toward wireless monitoring of intracranial pressure," *IEEE Microw. Wireless Compon. Lett.*, vol. 26, no. 7, pp. 549–551, Jul. 2016.
- [6] S. Rodriguez, S. Ollmar, M. Waqar, and A. Rusu, "A batteryless sensor ASIC for implantable bio-impedance applications," *IEEE Trans. Biomed. Circuits Syst.*, vol. 10, no. 3, pp. 533–544, Jun. 2016.
- [7] C. Li et al., "A noncontact wireless passive radio frequency (RF) resonant pressure sensor with optimized design for applications in high-temperature environments," Meas. Sci. Technol., vol. 25, no. 7, p. 075101, 2014.
- [8] Q. Tan et al., "A harsh environment-oriented wireless passive temperature sensor realized by LTCC technology," Sensors, vol. 14, no. 3, pp. 4154–4166, 2014.

- [9] H. Kairm et al., "Concept and model of a metamaterial-based passive wireless temperature sensor for harsh environment applications," *IEEE Sensors J.*, vol. 15, no. 3, pp. 1445–1452, Mar. 2015.
- [10] C. Li, Q. Tan, C. Xue, W. Zhang, Y. Li, and J. Xiong, "A high-performance LC wireless passive pressure sensor fabricated using low-temperature co-fired ceramic (LTCC) technology," *Sensors*, vol. 14, no. 12, pp. 23337–23347, Dec. 2014.
- [11] P.-J. Chen, S. Saati, R. Varma, M. S. Humayun, and Y.-C. Tai, "Wireless intraocular pressure sensing using microfabricated minimally invasive flexible-coiled LC sensor implant," *J. Microelectromech. Syst.*, vol. 19, no. 4, pp. 721–734, Aug. 2010.
- [12] U. Kawoos, X. Meng, M. R. Tofighi, and A. Rosen, "Too much pressure: Wireless intracranial pressure monitoring and its application in traumatic brain injuries," *IEEE Microw. Mag.*, vol. 16, no. 2, pp. 39–53, Mar. 2015.
- [13] H. Huang, P.-Y. Chen, C.-H. Hung, R. Gharpurey, and D. Akinwande, "A zero power harmonic transponder sensor for ubiquitous wireless μL liquid-volume monitoring," Sci. Rep., vol. 6, p. 18795, Jan. 2016.
- [14] E. Silavwe, N. Somjit, and I. D. Robertson, "A microfluidic-integrated SIW lab-on-substrate sensor for microliter liquid characterization," *IEEE Sensors J.*, vol. 16, no. 21, pp. 7628–7635, Nov. 2016.
- [15] Q. Y. Ren, L. F. Wang, J. Q. Huang, C. Zhang, and Q. A. Huang, "Simultaneous remote sensing of temperature and humidity by LC-type passive wireless sensors," *J. Microelectromech. Syst.*, vol. 24, no. 4, pp. 1117–1123, Aug. 2015.
- [16] X. Wang et al., "An all-printed wireless humidity sensor label," Sens. Actuators B, Chem., vol. 166, pp. 556–561, May 2012.
- [17] Y. Peng, B. F. Rahman, T. Wang, G. Wang, X. Liu, and X. Wen, "Characterization of a passive telemetric system for ISM band pressure sensors," *J. Electron. Test.*, vol. 30, no. 6, pp. 665–671, Dec. 2014.
- [18] M. H. Zarifi, T. Thundat, and M. Daneshmand, "High resolution microwave microstrip resonator for sensing applications," Sens. Actuators A, Phys. vol. 233, pp. 224–230, Sep. 2015.
- [19] M. H. Zarifi, S. Farsinezhad, K. Shankar, and M. Daneshmand, "Sensing using active feedback assisted planar microwave resonator," *IEEE Microw. Wireless Compon. Lett.*, vol. 25, no. 9, pp. 621–623, Sep. 2015.
- [20] M. Abdolrazzaghi, M. H. Zarifi, and M. Daneshmand, "Wireless communication in feedback-assisted active sensors," *IEEE Sensors J.*, vol. 16, no. 22, pp. 8151–8157, Nov. 2016.
- [21] C. M. Bender and S. Boettcher, "Real spectra in non-Hermitian Hamiltonians having PT symmetry," Phys. Rev. Lett., vol. 80, no. 24, p. 5243, Jun. 1998.
- [22] Z. Lin, H. Ramezani, T. Eichelkraut, T. Kottos, H. Cao, and D. N. Christodoulides, "Unidirectional invisibility induced by PTsymmetric periodic structures," Phys. Rev. Lett., vol. 106, no. 21, p. 213901, May 2011.
- [23] A. Regensburger et al., "Observation of defect states in PT-symmetric optical lattices," Phys. Rev. Lett., vol. 110, no. 22, p. 223902, May 2013.
- [24] A. Mostafazadeh, "Invisibility and PT symmetry," Phys. Rev. A, Gen. Phys., vol. 87, no. 21, p. 012103, Jan. 2013.
- [25] L. Feng et al., "Experimental demonstration of a unidirectional reflectionless parity-time metamaterial at optical frequencies," *Nature Mater.*, vol. 12, no. 2, pp. 108–113, Feb. 2013.
- [26] K. G. Makris, R. El-Ganainy, D. N. Christodoulides, and Z. H. Musslimani, "Beam dynamics in PT symmetric optical lattices," Phys. Rev. Lett., vol. 100, no. 10, p. 103904, Mar. 2008.
- [27] M. A. K. Othman, V. Galdi, and F. Capolino, "Exceptional points of degeneracy and PT-symmetry in photonic coupled chains of scatterers," Phys. Rev. B, Condens. Matter, vol. 95, no. 10, p. 104305, 2017.
- [28] C. E. Rüter, K. G. Makris, R. El-Ganainy, D. N. Christodoulides, M. Segev, and D. Kip, "Observation of parity-time symmetry in optics," *Nature Phys.*, vol. 6, no. 3, pp. 192–195, 2010.
- [29] J. M. Lee, S. Factor, Z. Lin, I. Vitebskiy, F. M. Ellis, and T. Kottos, "Reconfigurable directional lasing modes in cavities with generalized PT symmetry," Phys. Rev. Lett., vol. 112, no. 25, p. 253902, Jun. 2014.
- [30] H. Benisty et al., "Implementation of PT symmetric devices using plasmonics: Principle and applications," Opt. Express, vol. 19, no. 19, pp. 18004–18019, Sep. 2011.
- [31] R. Fleury, D. Sounas, and A. Alù, "An invisible acoustic sensor based on parity-time symmetry," *Nature Commun.*, vol. 6, p. 5905, Jan. 2015.
- [32] X. Y. Lü, H. Jing, J. Y. Ma, and Y. Wu, "PT-symmetry-breaking chaos in optomechanics," Phys. Rev. Lett., vol. 114, no. 25, p. 253601, Jun. 2015.
- [33] X.-W. Xu, Y.-X. Liu, C.-P. Sun, and Y. Li, "Mechanical PT symmetry in coupled optomechanical systems," Phys. Rev. A, Gen. Phys., vol. 92, no. 1, p. 013852, Jul. 2015.

- [34] L. Chang et al., "Parity-time symmetry and variable optical isolation in active-passive-coupled microresonators," *Nature Photon.*, vol. 8, no. 7, pp. 524–529, Jul. 2014.
- [35] D. M. Pozar, Microwave Engineering. Hoboken, NJ, USA: Wiley, 2009.
- [36] J. Schindler, A. Li, M. C. Zheng, F. M. Ellis, and T. Kottos, "Experimental study of active LRC circuits with PT symmetries," Phys. Rev. A, Gen. Phys., vol. 84, no. 4, p. 040101, 2011.
- [37] T. H. Lee, Planar Microwave Engineering: A Practical Guide to Theory, Measurement, and Circuits, vol. 1. Cambridge, U.K.: Cambridge Univ. Press, Aug. 2004.
- [38] M. Yazgi, A. Toker, and B. S. Virdee, "A new negative resistance circuit and an application for loss compensation in a distributed amplifier," *Analog Integr. Circuits Signal Process.*, vol. 60, no. 30, pp. 215–220, Sep. 2009.
- [39] B. Razavi, RF Microelectronics, vol. 2. Upper Saddle River, NJ, USA: Prentice-Hall, Jan. 1998.
- [40] B. Razavi, "The cross-coupled pair—Part III," IEEE Solid-State Circuits Mag., vol. 7, no. 1, pp. 10–13, Feb. 2015.
- [41] E. A. Vittoz, M. G. R. Degrauwe, and S. Bitz, "High-performance crystal oscillator circuits: Theory and application," *IEEE J. Solid-State Circuits*, vol. 23, no. 3, pp. 774–783, Jun. 1988.
- [42] M. Nick and A. Mortazawi, "Low phase-noise planar oscillators based on low-noise active resonators," *IEEE Trans. Microw. Theory Techn.*, vol. MTT-58, no. 5, pp. 1133–1139, May 2010.
- [43] Z. Chen, W. Hong, J. X. Chen, J. Zhou, and L. S. Li, "Low-phase noise oscillator utilising high-Q active resonator based on substrate integrated waveguide technique," *IET Microw., Antennas Propag.*, vol. 8, no. 3, pp. 137–144, Feb. 2014.
- [44] P. Y. Chen, C. Argyropoulos, and A. Alù, "Broadening the cloaking bandwidth with non-foster metasurfaces," *Phys. Rev. Lett.*, vol. 111, no. 23, p. 233001, Dec. 2013.
- [45] P. Y. Chen and J. Jung, "PT-symmetry and singularity-enhanced sensing based on photoexcited graphene metasurfaces," Phys. Rev. Appl., vol. 5, no. 6, p. 064018, Jun. 2016.
- [46] H. Hodaei et al., "Enhanced sensitivity at higher-order exceptional points," Nature, vol. 548, pp. 187–191, Aug. 2017.
- [47] H. Huang et al., "Chemical-sensitive graphene modulator with a memory effect for Internet-of-Things applications," *Microsyst. Nanoeng.*, vol. 2, p. 16018, May 2016.
- [48] M. S. Mannoor et al., "Graphene-based wireless bacteria detection on tooth enamel," Nature Commun., vol. 3, p. 763, Mar. 2012.



Maryam Sakhdari received the B.Sc. degree in electronics from the Iran University of Science and Technology, Tehran, Iran, in 2010, and the M.Sc. degree from Tarbiat Modares University in 2013. She is currently pursuing the Ph.D. degree with the Department of Electrical and Computer Engineering, University of Illinois at Chicago. Her doctoral work mainly focuses on low-noise harmonic transponder sensors, ultrasensitive PT-symmetric wireless sensors, electromagnetic metamaterials and plasmonics, and their RF, THz, infrared and optical applications.



Mehdi Hajizadegan received the M.Sc. degree in electronics from Tarbiat Modares University, Tehran, Iran, in 2013. He is currently pursuing the Ph.D. degree in electrical engineering with the Department of Electrical and Computer Engineering, University of Illinois at Chicago, where he is a Research Assistant. His research mainly focuses on graphene and other carbon-based biosensors, PT-symmetry-based wearable biosensors and leaky wave antennas, passive and active electromagnetic metamaterials and plasmonics, and their applications for energy harvesting.



Yue Li was a Visiting Scholar with the Department of Electrical and Systems Engineering, University of Pennsylvania. He is an Associate Professor with the Department of Electronic Engineering, Tsinghua University, Beijing, China. His research interests span over a broad range of antenna and metamaterial related areas, including epsilon-near-zero metamaterials, metamaterial-inspired circuits, optical nanocircuits and nanoantennas, mobile and handset antennas, diversity and MIMO antennas, reconfigurable antennas, mmw antennas and arrays, and beam forming and steering.



Jonathan C. H. Hung (M'15) received the B.S. degree from National Chiao-Tung University, Hsinchu, Taiwan, in 2001, the M.S. degree in electronic engineering from National Taiwan University, Taipei, Taiwan, in 2003, and the Ph.D. degree in electrical and computer engineering from the University of Texas at Austin in 2015. From 2003 to 2009, he was a Design Engineer at Taiwan Semiconductor Manufacturing Company, Hsinchu, in embedded DRAM and RF circuit design. Since 2014, he has been a Principal Member of Technical

Staff at Maxim Integrated Inc., leading a team engaged in the developments of low-power RFIC. His research interests include mixed-signal, analog, and RF integrated circuits.



**Mark Ming-Cheng Cheng** is an Associate Professor with the Department of Electrical and Computer Engineering and the Department of Biomedical Engineering, Wayne State University.



Pai-Yen Chen (S'09–M'13–SM'17) received the Ph.D. degree from the University of Texas at Austin in 2013. He is an Associate Professor with the Department of Electrical and Computer Engineering, University of Illinois at Chicago. He has been involved in multidisciplinary research on applied electromagnetics, wireless telemetry sensors, integrated micro/nano-sensor systems, and nano-optoelectronics, including plasmonics and nanophotonics.